VOLUME 111, NUMBER 5
MARCH 1, 1989

JOURNAL
OF THE
AMERICAN
CHEMICAL
SOCIETY

Vibrational Structure of the ^1L_b Transition of 1,6:8,13-Ethano[14]annulene. Transannular Interaction, the "Mystery Band", and the Kekulē Vibration

Kenneth A. Klingensmith,[1a,b] Harry J. Dewey,[1a] Emanuel Vogel,[1c] and Josef Michl*,[1a,b]

Contribution from the Department of Chemistry, University of Utah, Salt Lake City, Utah 84112, and Institut für Organische Chemie, Universität zu Köln, 5000 Köln 41, Greinstrasse 4, West Germany. *Received December 22, 1987*

Abstract: Resolved single-site selected fluorescence excitation spectra for the first excited singlet state (^1L_b) of 1,6:8,13-ethano[14]annulene and its deuterated analogue matrix-isolated in solid nitrogen are reported. When molecular mechanics and the PPP formalism for the ground-state force field and INDO/S calculations for the excitation energy are utilized, an approximate harmonic force field for the ^1L_b state is obtained. Calculated Franck–Condon factors permit an assignment of the previously unassigned "mystery band" ("A band") as a part of the fine structure of the ^1L_b band built on a false origin provided by two quanta of the "Kekulē" vibration. They also account for the observed long progression in a low-frequency vibration, highly unusual for an aromatic molecule. This is assigned to bridge bending, which strongly modulates the magnitude of transannular interaction.

Several separate investigations have dealt with the changes in molecular bonding within the progression from a purely cyclic annulene to a catacondensed polyacene.[2-6] In particular, a series of bridged [14]annulenes has provided a range of intermediate geometries wherein the transannular interaction, planarity, and degree of bond twisting vary smoothly.[2] The low-energy region of the absorption spectra (Figure 1) of these compounds contains four well-characterized transitions into the ^1L_b, ^1L_a, ^1B_b, and ^1B_a states of Platt[7] and up to three additional spectral features, provisionally labeled A–C and assigned as separate transitions.[2] These cannot be readily attributed to single π-electron excitations from the ground state. Calculations have suggested that a σ–π* excitation whose energy is lowered by hyperconjugation can account for the weak B band, which appears to be present only in 1,6:8,13-cyclopropano[14]annulene, and support for this assignment was found in a comparison with dicyclohepta[*cd*,*gh*]pentalene.[2] The intense C band has not found a convincing explanation so far, although inclusion of extensive configuration interaction places multiply excited states in the proper energy range, albeit with no intensity.[2,3] Massive vibronic intensity borrowing would have to be invoked for these states to acquire sufficient intensity to account for the observed spectrum. It is at least equally likely that the ^1L_a state borrows vibronic intensity to account for the observed C band.[6]

The third, weakest, and lowest energy band of the three, the A band, has found no explanation in terms of the perimeter model nor in semiempirical theory. The low energy of this band would seem to preclude an assignment to a σ-electron excitation: it is not reproduced by CNDO/S calculations.[8] No multiply excited states have been predicted to fall in this region, and the spectral shape and polarization make an assignment to vibronic borrowing appear highly improbable. An analogous band was observed for the first time two decades ago in a [10]annulene[9] and has by now

(1) (a) University of Utah. (b) Present Address: Center for Structure and Reactivity, Department of Chemistry, University of Texas at Austin, Austin, TX 78712-1167. (c) University of Cologne.
(2) Kolc, J.; Michl, J.; Vogel, E. *J. Am. Chem. Soc.* **1976**, *98*, 3935.
(3) Spanget-Larsen, J.; Gleiter, R. *Helv. Chim. Acta* **1978**, *61*, 2999.
(4) Dewey, H. J.; Deger, H.; Frölich, W.; Dick, B.; Klingensmith, K. A.; Hohlneicher, G.; Vogel, E.; Michl, J. *J. Am. Chem. Soc.* **1980**, *102*, 6412.
(5) Klingensmith, K. A.; Püttmann, W.; Vogel, E.; Michl, J. *J. Am. Chem. Soc.* **1983**, *105*, 3375.
(6) Borsch-Pulm, B.; Demmer, M.; Murthy, P. S.; Lex, J.; Schieb, E.; Vogel, E.; Hohlneicher, G.; Michl, J. *J. Phys. Chem.* **1987**, *91*, 1382.
(7) Platt, J. R. *J. Chem. Phys.* **1949**, *17*, 484. Moffitt, W. *J. Chem. Phys.* **1954**, *22*, 1820.
(8) Dick, B.; Hohlneicher, G. *Theor. Chim. Acta* **1979**, *53*, 221.

0002-7863/89/1511-1539$01.50/0

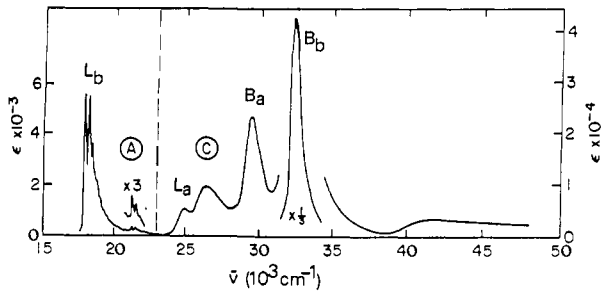

Figure 1. Room-temperature absorption spectrum of **1** in 3-methylpentane. Reproduced by permission from ref 2.

Table I. Experimental Vibrational Frequencies in the ^1L_b Band of **1** and **1**-d_{10} (cm^{-1})

1 (origin: 18 032)	**1**-d_{10} (origin: 18 081)	**1** (origin: 18 032)	**1**-d_{10} (origin: 18 081)
0	0	804	777
109	108		1019
236	218	1117	1055
401	387		1150
	390		1195
	469		1359
596	548		1550
	706		

acquired the reputation of a "mystery" band.

We now report the results of an examination of matrix-isolated 1,6:8,13-ethano[14]annulene (**1**) and **1**-d_{10}, deuterated in all

1

aromatic positions, using single-site selected fluorescence excitation spectroscopy[10] (Table I). This technique selects a narrow range of sites from an inhomogeneous spectral distribution profile in a low-temperature sample by using a narrow bandwidth excitation beam for scanning and observing only a narrow wavelength range in emission. When only a restricted population in emission is observed, it is possible to remove some of the inhomogeneous broadening and to untangle the spectral congestion due to multiple sites (Figure 2). In our case, peaks due to individual sites are clearly apparent in the ordinary absorption and emission spectra, and selecting a particular peak for observation is relatively straightforward. The site-selected spectra of **1** and **1**-d_{10} in solid nitrogen show highly resolved vibrational structure for the first 5000 cm^{-1} above the electronic origin of the lowest energy transition. Inspection of these, of the analogous results for **1**-d_{10}, and comparison with the calculated Franck–Condon factors for the transition permit several conclusions to be made. All observed features are accounted for, including a very dominant progression in a low-frequency vibration and the origin of the previously unassigned A band. Some of the present results, including a less definitive assignment of the A band, have been reported in a preliminary communication.[11]

Experimental Part

Sample Preparation. A sample of **1**-d_{10} was obtained from **1**[2] by treatment with a 2:1 solution of CF_3COOD in $DCCl_3$ under an argon atmosphere for several days at room temperature. NMR spectroscopy showed the sample to be 95% labeled in the conjugated perimeter and the unexchanged hydrogens to be on the bridge. Vacuum sublimation at 90 °C for 2 days afforded spectroscopically pure **1**-d_{10}.

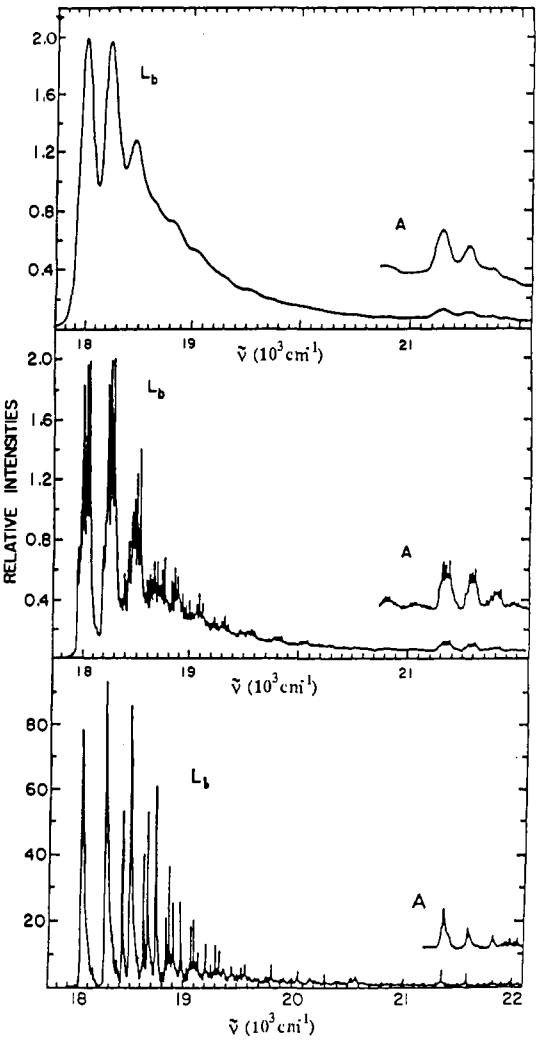

Figure 2. Absorption spectrum of **1**. Top: **1** in 3-methylpentane glass at 77 K. Center: Excitation spectrum of **1** matrix isolated in nitrogen at 14 K. Bottom: Single-site selected fluorescence excitation spectrum of **1** matrix isolated in nitrogen at 14 K. Reproduced by permission from ref 11.

Spectroscopy. Polarized IR spectra were measured on a sample of **1** imbedded in stretched polyethylene by using the techniques of ref 12. Fluorescence measurements were performed on the nitrogen-pumped dye laser system described elsewhere.[11] An Air Products CS-202 Displex closed-cycle cryostat was used for matrix isolation. For deposition, the sample of **1** or **1**-d_{10} was held at 80 °C to maintain sufficient vapor pressure for a high-quality matrix. Nitrogen flow rates of 1 mmol/min for 2 h deposited on a sapphire window held at 27 K generally produced transparent matrices of approximmely 2-mm thickness. Some matrix cracking was observed when the temperature was subsequently lowered to 14 K; however, light scattering was still quite low. Optical densities were kept at 0.1 or less, such that a low sample concentration was maintained to avoid energy transfer that would increase the number of sites monitored and distort the polarization information obtained by photoselection. This also ensured that the excitation spectra were valid representations of the corresponding absorption spectra. An estimate of the sample concentration assuming the worst case [absorbance 0.1, 1-mm path length, ϵ (solution, RT) = 8 × 10^4] is 1.25 × 10^{-5} M.[4]

The single-site selected fluorescence excitation spectrum of the low-energy region of matrix-isolated **1** is shown in Figure 2. The fluorescence monitoring wavelength was chosen to minimize the spectral bandwidth of the observed excitation profiles and the site contamination in the spectrum. In all spectra, the instrumental resolution was determined by the analyzing monochromator and was just sufficient to define the spectral line shapes (approximately 0.2 Å, i.e., 0.7 cm^{-1} at 5500 Å). The narrowest line widths measured were not less than 1.5 Å (fwhm).

(9) Blattmann, H.-R.; Boekelheide, V.; Heilbronner, E.; Weller, J.-P. *Helv. Chim. Acta* **1967**, *50*, 68.
(10) Personov, R. J.; Kharlamov, B. M. *Opt. Commun.* **1973**, *7*, 417. Bykovskaya, L. A.; Personov, R. J.; Kharlamov, B. M. *Chem. Phys. Lett.* **1974**, *27*, 80.
(11) Dewey, H. J.; Michl, J. *J. Lumin.* **1981**, *24*, 527.
(12) Radziszewski, J. G.; Michl, J. *J. Phys. Chem.* **1981**, *85*, 2934; *J. Chem. Phys.* **1985**, *82*, 3527; *J. Am. Chem. Soc.* **1986**, *108*, 3289.

The symmetry of the vibrations was determined from measurements of fluorescence polarization. The relative orientation of the absorption and emission transition moments is determined by the measurement of the polarized emission intensities parallel ($I_\parallel$) and perpendicular ($I_\perp$) to the polarization direction of the exciting light. The degree of polarization is defined as $P = (I_\parallel - I_\perp)/(I_\parallel + I_\perp)$. For parallel transition moment directions, $P = {}^1/_2$, while for perpendicular transition moment directions, $P = -{}^1/_3$. All vibrational lines were observed to be polarized parallel to the band origin ($0.4 < P < 0.5$). The region located half-way between the ^1L_b origin and the origin of the A band was examined particularly carefully for the presence of weak perpendicularly polarized peaks, but none were found.

A weak A band analogue in the emission of **1** has been observed at 3060 cm^{-1} relative to the origin.[11] An intensive search for the corresponding feature in **1**-d_{10} was unsuccessful.

Results

Calculations. In the bridged [14]annulenes such as **1**, the electric dipole moment of the transition from the ground state to the first excited singlet state has a moderate size, and the peaks of the vibrational fine structure are found to be polarized parallel to the origin. The electric dipole transition moment is known to be oriented along the molecular long axis and corresponds to the ^1L_b band in the cyclic parent annulene.[4] It is unlikely that significant intensity is borrowed vibronically through totally symmetric vibrations since even the nearest available intense long-axis polarized electronic state is separated by an energy gap of about 15 000 cm^{-1}. Thus, a spectral simulation can be accomplished by assuming the purely electronic transition dipole moment to remain constant throughout the ^1L_b electronic band and the fine structure to be related to the Franck–Condon overlap between the initial and final vibronic states

$$|\langle Ff|\mathbf{M}|Gg\rangle|^2 = |\langle F|\mathbf{M}|G\rangle|^2|\langle f|g\rangle|^2 \qquad (1)$$

where $|Ff\rangle$ is the fth vibrational state in the Fth electronic state, $|Gg\rangle$ is the ground vibrational level of the ground electronic state, $\mathbf{M}$ is the total electric dipole moment operator, broken brackets denote integration over the electronic coordinates, and parentheses denote integration over nuclear coordinates. With $\langle F|\mathbf{M}|G\rangle$ assumed constant, the problem reduces to the determination of ground- and excited-state vibrational wave functions and the integration over nuclear coordinates.

Ground State. The size and complexity of the structure **1** dictated the choice of methodology in the vibrational wave-function determination. Molecular mechanics has been shown capable of accurate structural representation of known molecular X-ray structures of a wide variety of hydrocarbons[13] and, in particular, of the structures of several bridged [10]- and [14]annulenes.[14] We have modified the program BGSTRN-2[15] in a way to maintain consistency for the bridged [14]annulenes rather than use available programs that have been parametrized for vibrations.[16] Factors related to geometry will be better represented than those related to vibrational frequencies. Incorporation of delocalized bonding forces necessary for an extended conjugated system such as **1** was accomplished using the relationships[14,17,18] (in units of kilocalories per mole and angstroms)

$$E(r) = (1/2)k(r - r_0)^2$$

$$k = 5.0 + 4.6p_{ij}$$

$$r_0 = 1.511 - 0.179p_{ij}$$

$$2E(\alpha) = V_1(1 + \cos\alpha) + V_2(1 - \cos 2\alpha)$$

$$V_1 = 1; \qquad V_2 = 54.2p_{ij}^2/4 \qquad (2)$$

Table II. Geometry of **1**

structural param[a]	obsd[19,b]	calcd[c]	calcd[17]
	Distances, Å		
C_1–C_2	1.406	1.414	1.401
C_2–C_3	1.382	1.392	1.404
C_3–C_4	1.404	1.420	1.409
C_1–C_{14}	1.387	1.398	1.396
C_1–C_{15}	1.524	1.487	1.491
C_{15}–C_{16}	1.570	1.529	1.536
	Angles, deg		
C_1–C_2–C_3	127.0	125.6	124.7
C_2–C_3–C_4	128.3	129.9	128.5
C_5–C_6–C_7	127.3	127.7	125.1
C_6–C_7–C_8	112.8	109.2	108.8
C_2–C_1–C_5	123.3	121.7	123.6
C_1–C_{15}–C_6	108.2	117.9	110.1
C_1–C_{15}–C_{16}	104.1	104.6	104.0
torsion C_1–C_2	23	17	16
torsion C_2–C_3	16	14	19
torsion C_3–C_4	1.4	0.0	0.1
torsion C_6–C_7	8	7	7

[a] Torsion defined as the dihedral angle between the $2p_z$ orbitals located on the two atoms indicated. [b] X-ray structure. [c] Present work.

Table III. Steric Energy Analysis for **1** (kcal/mol)

interaction	ref 17	this work
stretch	1.97	0.27
bend	11.34	17.08
twist	16.33	37.79
nonbonded	18.21	4.71
stretch–bend	−0.46	−0.11
total	47.39	58.75

where the bond order p_{ij} between atoms i and j is calculated within the Pariser–Parr–Pople formalism[19] and α is the twist angle. The transannular interaction that occurs in bridged annulenes was incorporated into the PPP calculation as a resonance integral between the 1–6 and 8–13 carbons of the perimeter with 40% the value of the resonance integral of benzene.[4,5,9] The factors cos α account for the nonplanarity of the molecules. Changes in the mathematical form of $E(\alpha)$ had little or no effect on the calculated geometry of **1**. Any effects invariably were in the direction of increased transannular distance and equalized annulene bond lengths relative to those listed here.

The structural parameters obtained for **1** very closely approximate the reported X-ray structure[20] (Table II). The C_{2v} symmetry and bond-length alternation in the aromatic framework are well represented, while the saturated bonds of the bridge are shorter than they should be. Also the bond angles and torsions are all reproduced fairly well, except that the bridge CCC angle controlling the transannular distance is opened up from 108.2° to 117.9°. This suggests that by allowing this angle to open the associated saturated bonds shorten. Comparison with a previous calculation,[17] which utilized a slightly different torsional potential, indicates that this is indeed so (Table II) and that the relationships between the bond order and force constants perhaps overestimate the importance of delocalization. This can be clearly seen in a comparison of strain energies, tabulated in Table III. Most of the strain energy resides in the torsions, with a smaller amount in the stretches.

The frequencies calculated from the molecular mechanics force field are listed by symmetry group in Tables IV and V. Also listed are the results of polarized IR measurements on **1** partially aligned in a stretched polyethylene sheet and single-site selected fluorescence frequencies from a matrix-isolated sample.

(13) Allinger, N. L. *Adv. Phys. Org. Chem.* **1976**, *13*, 1; *J. Am. Chem. Soc.* **1977**, *99*, 8127. Burkert, U.; Allinger, N. L. In *Molecular Mechanics*; American Chemistry Society: Washington, DC, 1982.
(14) Favini, G.; Simonetta, M.; Todeschini, R. *J. Comput. Chem.* **1981**, *2*, 149.
(15) Iverson, D. J.; Mislow, K. *QCPE* **1981**, *13*, 410.
(16) Warshel, A.; Levitt, M. *QCPE* **1982**, *13*, 247.
(17) Favini, G.; Simonetta, M.; Sottocornola, M.; Todeschini, R. *J. Chem. Phys.* **1981**, *74*, 3953.
(18) Allinger, N. L.; Sprague, J. T. *J. Am. Chem. Soc.* **1973**, *95*, 3893.
(19) Pariser, R.; Parr, R. G. *J. Chem. Phys.* **1953**, *21*, 466, 767. Pople, J. A. *Trans. Faraday Soc.* **1953**, *49*, 1375.
(20) Bianchi, R.; Casalone, G.; Simonetta, M. *Acta Crystallogr., Sect. B* **1967**, *33*, 1207.

Table IV. Ground-State Vibrations[a] of **1**: b_1 and b_2 Symmetry (cm^{-1})

b_1			b_2		
obsd[b]	no.	calcd	obsd[b]	no.	calcd
	19	198		19	213
	18	214		18	282
	17	401		17	393
505	16	444		16	500
561	15	554	612	15	566
660	14	628	648	14	666
677	13	746	757	13	722
863	12	842	765	12	805
896	11	884	838	11	830
948	10	970	924	10	866
963	9	1072	975	9	887
1245	8	1208	1015		
	7	1412	1051		
	6	1458	1078		
	5	1488	1107		
1805	4	1795	1149	8	1152
	3	2846	1225		
	2	2872	1255	7	1255
	1	2903	1296		
			1306		
				6	1458
			1529		
			1563		
			1820		
				5	1756
				4	1911
			1918		
			1930		
			2048		
				3	2848
				2	2857
				1	2872

[a] The correspondence of calculated to observed frequencies is based on close matching of experimental and calculated frequencies of identical symmetry. [b] Experimental frequencies obtained from the room-temperature polarized IR spectrum of **1** embedded in stretched polyethylene. The lower wavenumber limit is determined by the spectrometer optics and detector used.

Table V. Ground-State Vibrations of **1**: a_1 Symmetry (cm^{-1})

obsd		calcd	
IR[a]	fluorescence[b]	no.	vibration
		22	100
	231	21	194
		20	282
	383	19	341
	411	18	478
603	602	17	547
691	655	16	652
739	747	15	706
777	769	14	734
813	839	13	834
822		12	866
880		11	1071
911		10	1182
960			
1005			
1208	1219	9	1209
1230		8	1262
1318		7	1414
1342			
	1719	6	1639
	1831		
	2012	5	1892
	2131		
		4	2894
		3	2857
		2	2872
		1	2903

[a] Room-temperature polarized IR of **1** embedded in stretched polyethylene. [b] Single-site selected fluorescence of **1** matrix isolated in nitrogen at 14 K.

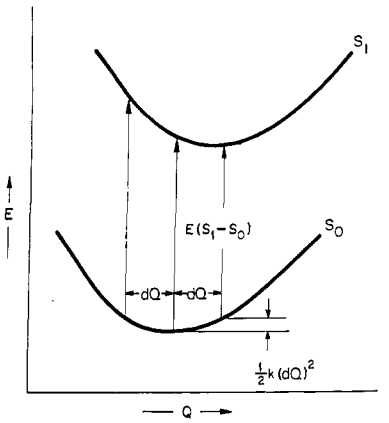

Figure 3. Construction of the harmonic approximation to the lowest excited singlet potential surfaces.

First Excited State. In $\pi-\pi^*$ excited states overall π-electron bonding will decrease and the vibrational potentials relax as electron density is promoted from bonding into antibonding MO's. This gives rise to the normally observed decrease in vibrational frequencies upon excitation of the ground state to the first excited singlet state. As the transannular distance is kept artificially long in this force field by the overemphasized delocalization energy, in the excited state one can expect it to decrease significantly due to the loss of π-electron-induced skeletal rigidity.

The excited-state potential function may be constructed from the ground electronic state potential assuming harmonic force fields and an absence of Dushinsky rotation[21] as diagrammed in Figure 3. This neglect of the possible mixing of normal modes in the excited state is supported by the approximate mirror image between the excitation and fluorescence spectra.[11] Distortion of the molecule along a specific normal mode a distance Q from the ground-state equilibrium geometry position Q_0 will increase the ground-state energy by $(1/2)k(Q - Q_0)^2$ as given by the ground-state harmonic force constant k. The transition energy from the ground to the excited state is calculated by the INDO/S method.[22] At least some configuration interaction is mandatory, but it can be quite limited since even in extensive CI wave functions for **1** the lowest singlet state ^1L_b is well represented by the configurations obtained by single-electron promotions from the HOMO to the second LUMO and from the second HOMO to the LUMO. This was verified by inspection of the eigenvectors of a CI matrix with all singly excited configurations calculated at the equilibrium geometry. In addition, the CI eigenvectors were followed during vibrational distortions to guard against large changes in configurational contributions to ^1L_b. None were observed. INDO/S calculation of the transition energy of the ^1L_b band at the ground-state equilibrium geometry gave an excitation energy of 17 790 cm^{-1}, to be compared with the experimental energy of 18 032 cm^{-1}. At several geometries along each normal mode, the calculated excitation energy was added to the increase in ground-state energy obtained as described above to create a representation of the ^1L_b potential surface along that particular normal mode. The set of excited-state energies obtained in this manner were fitted to the function

$$E(S_1) = E_0 + (1/2)k'(Q - Q'_0)^2 \quad (3)$$

where E_0 is the 0–0 transition energy, k' is the excited-state force constant, and Q is the displacement along the normal mode from the excited electronic state equilibrium position Q'_0 for that particular normal mode.

Franck–Condon Factors. The calculation of Franck–Condon factors is greatly simplified as at 14 K the initial vibrational state can be assumed to be the ground vibrational state. In addition, in the absence of Dushinsky rotation the same reduced mass is maintained in a normal mode in both electronic states. The

(21) Dushinsky, F. *Acta Physicochim. USSR* **1937**, *7*, 551.
(22) Zerner, M.; Ridley, J. *Theor. Chim. Acta* **1973**, *32*, 111.

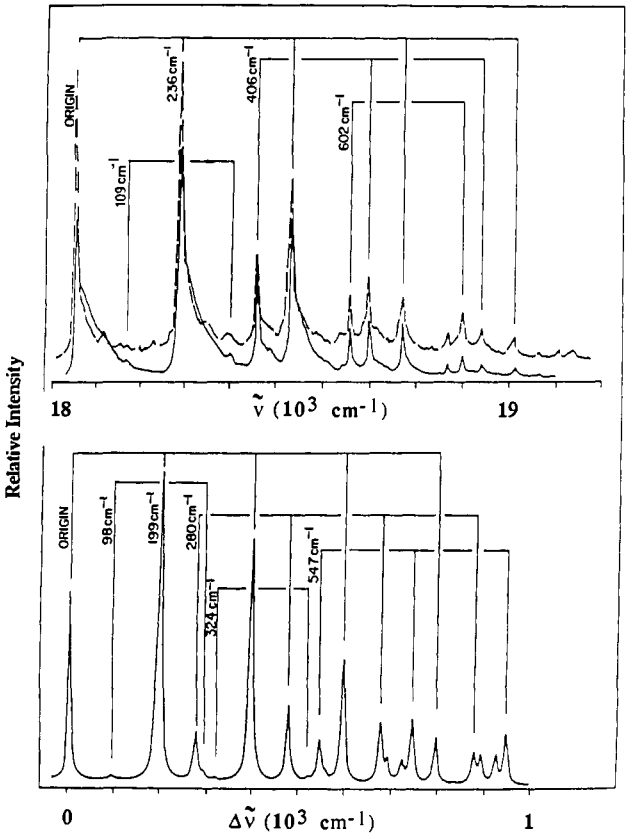

Figure 4. Low-energy excitation spectrum of **1**. Top: Full, single-site selected fluorescence excitation spectrum of **1** matrix isolated in nitrogen at 14 K (dashed, the "A band", shifted by 3320 cm^{-1} to lower frequencies to align its origin with the ^1L_b origin). Bottom: Simulated absorption spectrum of **1**.

Franck–Condon factors $|(0|n)|^2$ have been calculated using the relations[23]

$$|(0|n)|^2 = |(0|0)|^2\ (a/2)^n\ |H_n(ix)|^2/n!$$
$$|(0|0)|^2 = (1 - a^2)^{1/2} \exp(-b)$$
$$a = (\tilde{\nu} - \tilde{\nu}')/(\tilde{\nu} + \tilde{\nu}')$$
$$b = (kk')^{1/2}(q' - q)^2/[(h/2\pi)(\tilde{\nu} + \tilde{\nu}')] \qquad (4)$$
$$x = [b(1 - a)/2a]^{1/2}$$

where $\tilde{\nu}$, k, and q fully specify the harmonic oscillator wave function, and prime denotes the upper state. $H_n(ix)$ is a Hermite polynomial of an imaginary argument. Table VI lists the calculated frequencies and Franck–Condon intensities for the transition from the ground state to the first excited singlet state for totally symmetric and nontotally symmetric vibrations of **1**. Table VII lists the analogous values for **1**-d_{10}. Only those with significant intensity in lines other than the origin are listed.

Spectral Simulation. The simulated spectra shown in Figures 4–6 are based on the calculated frequencies and Franck–Condon intensities

$$I(\tilde{\nu}) = \prod_n \prod_m |(0|\tilde{\nu}_m^n)|^2 L(\tilde{\nu}, \tilde{\nu}_m^n, w) \qquad (5)$$

where $L(\tilde{\nu}, \tilde{\nu}_m^n, w)$ is the Lorentzian line-shape function dependent on $\tilde{\nu}$, centered at the nth quantum of the mth fundamental $\tilde{\nu}$, and width w:

$$L(\tilde{\nu}, \tilde{\nu}_m^n, w) = w/\{2\pi[(\tilde{\nu} - \tilde{\nu}_m^n)^2 + (w/2)^2]\} \qquad (6)$$

The simulations used line widths of 10 cm^{-1} in **1** and 5 cm^{-1} in **1**-d_{10} to match those observed.

Discussion

Spectral Features. The long-wavelength part of the spectrum is composed of the ^1L_b origin at 18 032 cm^{-1} (**1**-d_{10}, 18 081 cm^{-1}) and of many well-defined additional lines falling into three main categories: (i) a few corresponding to a single quantum of a totally symmetric vibration; (ii) a strong and long progression in a totally symmetric 236-cm^{-1} vibration (**1**-d_{10}, 218 cm^{-1}) building on other

(23) Siebrand, W. *J. Chem. Phys.* **1967**, *46*, 440.

Table VI. Calculated Franck–Condon Factors of **1**[a]

Totally Symmetric Vibrations

no.	$\tilde{\nu}$	$\tilde{\nu}'$	ΔQ	$\lvert(0\lvert1)\rvert^2/\lvert(0\lvert0)\rvert^2$
22	100	98	−0.073	0.24
21	194	199	0.306	4.00
20	282	280	−0.040	0.24
19	341	324	−0.009	0.01
18	478	474	0.004	0.0
17	547	547	0.040	0.20
15	706	694	0.025	0.08
14	734	726	0.019	0.08
10	1182	1180	−0.002	0.0
9	1209	1202	−0.002	0.0
8	1262	1260	0.002	0.0
7	1414	1412	−0.004	0.01
5	1892	1905	−0.003	0.01

Nontotally Symmetric Vibrations

sym	no.	$\tilde{\nu}$	$\tilde{\nu}'$	$10^3\lvert(0\lvert2)\rvert^2/\lvert(0\lvert0)\rvert^2$
b_1	18	214	208	0.01
a_2	15	377	366	0.13
b_1	16	444	426	0.20
a_2	12	719	692	0.19
b_1	13	746	725	0.11
b_2	4	1911	2060	0.71

[a] Calculated energies in the ground (ν) and excited (ν') state (cm^{-1}); ΔQ is the normal-mode coordinate displacement between harmonic minima.

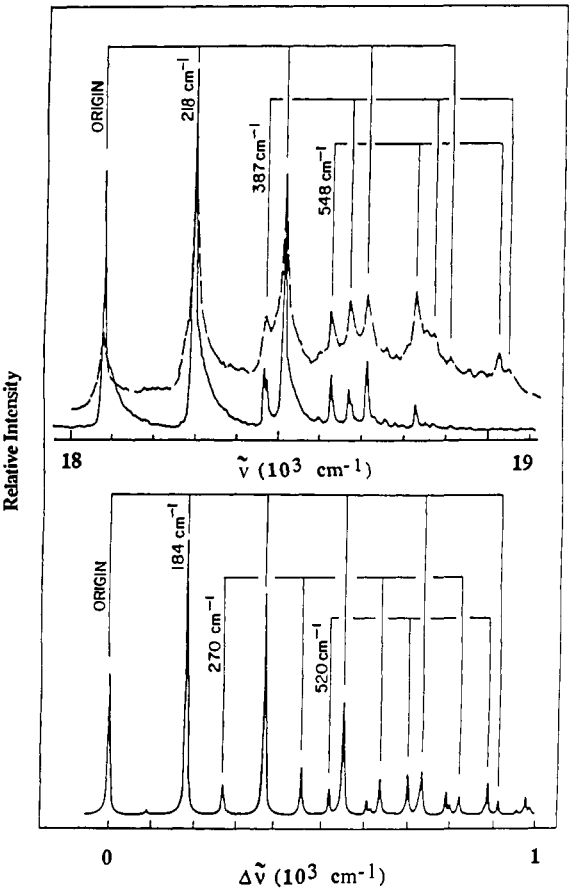

Figure 5. Low-energy excitation spectrum of **1**-d_{10}. Top: Full, single-site selected fluorescence excitation spectrum of **1**-d_{10} matrix isolated in nitrogen at 14 K (dashed, the A band, shifted by 3300 cm^{-1} to lower frequencies to align its origin with the ^1L_b origin). Bottom: Simulated absorption spectrum of **1**-d_{10}.

Table VII. Calculated Franck–Condon Factors of **1**-d_{10}[a]

Totally Symmetric Vibrations

no.	$\tilde{\nu}$	$\tilde{\nu}'$	ΔQ	$\lvert(0\lvert1)\rvert^2/\lvert(0\lvert0)\rvert^2$
22	94	92	0.070	0.24
21	180	184	−0.287	6.00
20	272	270	−0.032	0.16
19	318	304	0.006	0.0
18	458	455	−0.004	0.0
17	471	467	−0.004	0.0
16	520	520	−0.031	0.14
15	549	546	−0.020	0.06
14	609	608	−0.015	0.07
10	619	619	−0.009	0.03
9	699	696	0.006	0.01
8	959	957	0.006	0.02
7	1043	1043	−0.003	0.01
6	1382	1381	−0.003	0.01
5	1882	1894	−0.003	0.01

Nontotally Symmetric Vibrations

sym	no.	$\tilde{\nu}$	$\tilde{\nu}'$	$10^3\lvert(0\lvert2)\rvert^2/\lvert(0\lvert0)\rvert^2$
a_2	15	359	349	0.11
b_1	16	414	399	0.16
a_2	14	495	480	0.11
b_2	4	1905	2056	0.73

[a] Calculated energies in the ground (ν) and excited (ν') state (cm^{-1}); ΔQ is the normal-mode coordinate displacement between harmonic minima.

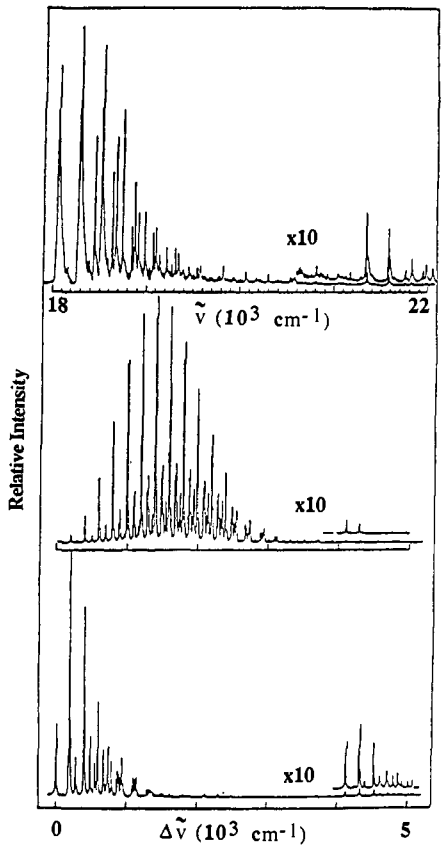

Figure 6. Excitation spectrum of **1**. Top: Single-site selected fluorescence excitation spectrum of **1** matrix isolated in nitrogen at 14 K. Center: Simulated absorption spectrum of **1**. Bottom: Simulated absorption spectrum of **1**, adjusted.

vibrations as false origins; (iii) and the mystery band A, an unexpectedly intense and distinct replica of the region near the origin, shifted 3320 cm^{-1} (**1**-d_{10}, 3300 cm^{-1}) above the electronic origin.

The identical nature of the vibrations built on the ^1L_b origin and those built on the origin of the A band, located 3320 cm^{-1} (**1**-d_{10}, 3300 cm^{-1}) higher is demonstrated in Figure 4 for **1** and Figure 5 for **1**-d_{10}. Several common vibrations are observed in the main ^1L_b body and in the A band, and on each of these a progression is built in a low-frequency vibration. This progression in both **1** and **1**-d_{10}, at 236 and 218 cm^{-1}, respectively, reaches maximum intensity between the second and third quanta of energy and can be seen to tail out as far as the fifth quantum. The intensity distributions in the progressions based on false origins have a decreasing exponential nature. In addition, the separations of the individual members of the progressions become somewhat smaller as the number of quanta increases, evidence of anharmonicity in the vibration. We have not been able to determine the anharmonicity term in the vibration accurately. The difference between the first and the second quantum of the low-frequency vibration in **1** is about 5 cm^{-1}. Within the experimental resolution of the instrument, all details in the spectra of both **1** and **1**-d_{10} align themselves ideally when the ^1L_b electronic origin and the A band origin at 3320 cm^{-1} (**1**-d_{10}, 3300 cm^{-1}) are overlayed, even with respect to the intensity distributions (Figures 4 and 5). As is to be expected in the low-frequency range of these molecules, the vibrational frequencies do not vary much between **1** and **1**-d_{10}, and the gross spectral features of the two compounds are quite similar. The frequencies of the low-energy region of **1** and **1**-d_{10} are collected in Table I.

The simulation can be directly compared with the full 5000-cm^{-1} spectrum in Figure 6. The uncorrected simulation identifies the vibrations qualitatively. For quantitative aspects we can adjust the computed spectral intensity profiles and the frequencies, based on approximate theoretical force fields, to better represent the experimental spectra. Without such adjustment, several discrepancies are present that mask the similarity of the calculated spectrum with what is observed experimentally. First, the calculated frequencies are not accurate, and the entire spectrum is compressed. Second, the Franck–Condon forbiddenness with respect to the long progression is exaggerated. Third, the amount of intensity present in the fundamental at 98 cm^{-1} (**1**-d_{10}, 92 cm^{-1}) is too large in comparison with the observed spectra. Finally, the calculated intensity of the A band is too low.

The first three discrepancies are removed in Figures 4 and 5 by adopting the experimental frequencies and adjusting the coordinate displacement of the totally symmetric normal modes $22a_1$ and $21a_1$ to fit the measured intensity patterns. The last discrepancy is resolved by using the ratio of the intensities of the origin to that of the A band origin to estimate the ground-state frequency for the normal mode $4b_2$. The ratio is equal to $2\lvert(0\lvert2)\rvert^2/\lvert(0\lvert0)\rvert^2 = a^2$, where a has been defined in eq 4 and can be determined from the observed spectra to be about 0.045. A frequency shift factor $\tilde{\nu}/\tilde{\nu}' = (1 - a)/(1 + a)$ of 0.91 results. Assuming this value to be correct and approximating experimental frequency in the excited state by its harmonic value of 3320/2 cm^{-1} (**1**-d_{10}, 3300/2 cm^{-1}), the ground-state frequency is calculated at 1517 cm^{-1} (**1**-d_{10}, 1508 cm^{-1}). Two ground-state vibrations of b_2 symmetry are observed in the polarized IR of **1** in stretched polyethylene in this frequency region (Table IV). In fluorescence, the second quantum of this vibration would be expected to occur at 3034 cm^{-1} (**1**-d_{10}, 3016 cm^{-1}) in the harmonic approximation. The observed value of the difference between the origin and the A band analogue in fluorescence[11] is 3060 cm^{-1} in **1**; the A band analogue was too weak to be observed in **1**-d_{10}. The agreement for **1** is excellent and lends credence to the simple analysis: the Dushinsky effect indeed appears to be unimportant and anharmonicity is not excessive.

The resulting adjusted simulated spectra are reasonably similar to experiment, both in the low-energy vibrational frequency range (Figures 4 and 5) and in the region of the "A band". This is indeed well represented as a replica of the band at the origin, starting at a false origin based on the second quantum of the nontotally symmetric vibration $4b_2$. We propose that this clarifies the origin of the mystery band A.

Totally Symmetric Vibrations: The Low-Frequency Progression and Transannular Interaction. In general, the calculated Franck–Condon factors show no surprises. Most of the intensity resides in the electronic origin, with only a few totally symmetric

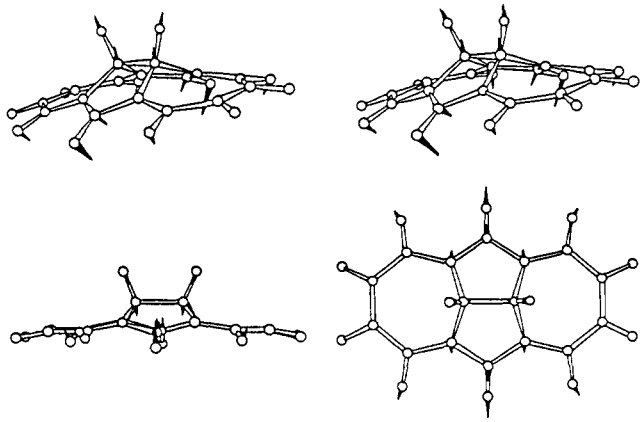

Figure 7. Normal mode $21a_1$. Top: Stereoview. Bottom: Top and side views. Darkened arrows represent atomic displacement vectors.

modes having the requisite intensity to be observed. No single vibration is calculated to undergo a significant frequency change upon excitation, thus for a totally symmetric vibration to have intensity the relative minima of the harmonic wells must be shifted.

This is observed in the calculations for only one mode, $21a_1$ at 194 cm^{-1} (**1**-d_{10}, 180 cm^{-1}). This vibration is unique among the calculated normal modes as being the only one that is Franck–Condon forbidden. Indeed, an exceptionally large displacement of harmonic minima shifts the maximum intensity to a higher quantum number than observed for any vibrational mode experimentally.

The Cartesian displacements in this mode are represented graphically in Figure 7. The vibration primarily involves a flattening of the molecule bringing together the ethano bridge and the plane roughly containing the annulene ring. Very small actual displacement of the transannular carbons 1, 6, 8, and 13 is evident. However, the motion of the bridge and of the adjacent 7 and 14 ring carbons modulates the $2p_z$ orbital directions by increasing the sp^2-bonding angles of these transannular carbons and thus the transannular overlap. The resonance integral between these carbons can be assumed to be approximately proportional to the overlap integral and is modulated during the course of the vibration. Distortion of the equilibrium geometry in the ground state by the mean-square displacement of normal mode $21a_1$ changes the bridge angle by nearly 2.5° (for a corresponding change in transannular distance of 0.25 Å). Taking into account the rehybridization of the orbitals located on the bridgehead carbons and the change in transannular distance, the modulation of the bridgehead carbon $2p_z$ orbital overlap can be estimated at 10%.

The reason for the large change in the equilibrium geometry along this normal mode is clear upon inspection of the MO's shown in Figure 8: a strongly stabilizing transannular interaction between the bridgehead carbons becomes much less stabilizing or even destabilizing in the excited state, and the transannular bond orders drop significantly. Configuration interaction spanning the full single excitation space at the PPP level calculates the ground-state transannular bond order at 0.30 with a decrease to 0.16 in the first excited state.

The previously described propensity of the force field to overemphasize stabilization by delocalization can explain why the calculated effect of the weakening of the transannular stabilization upon excitation would be particularly dramatic, exaggerating the shift of the equilibrium geometry along a vibrational coordinate that modulates the transannular interaction: skeletal relaxation in the first excited singlet state allows the bridgehead angle to close and relieve the strain.

We believe that the assignment of the unique progression-forming vibrational mode as the transannular interaction modulating flattening of the polycyclic system (Figure 7) is quite secure. It is suggested by the combined evidence of close numerical agreement between the calculated and the observed excited-state frequencies and a uniquely strong shift of intensity to high quanta in the calculated Franck–Condon envelope.

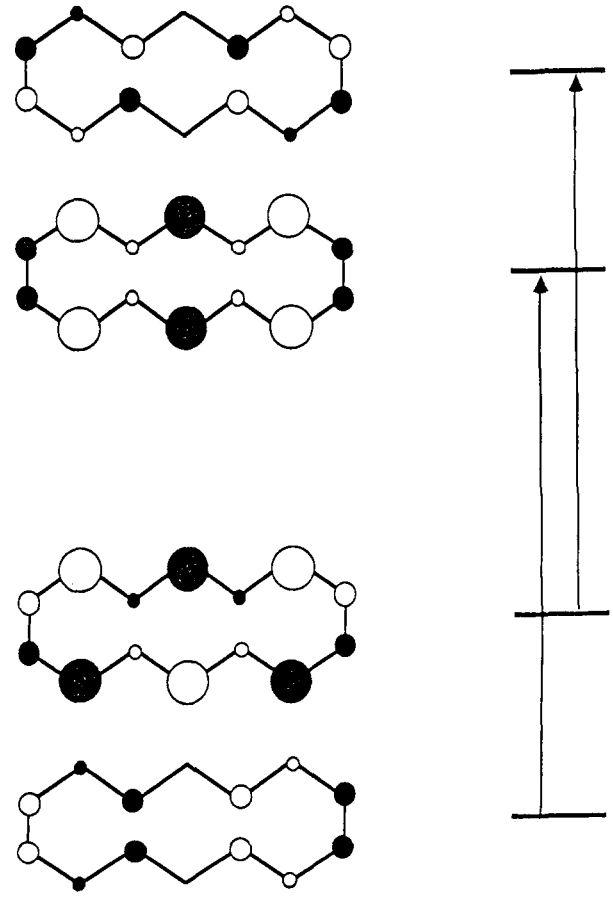

Figure 8. Frontier molecular orbitals of **1**.

It is likely that progressions in low-frequency vibrations that dominate the L_b bands of other methano-bridged annulenes are due to vibrations of similar nature, i.e., to normal modes that strongly modulate the transannular interaction. If this proposal is correct, it is thus the "homoaromatic" nature of these annulenes that is responsible for the striking appearance of their spectra, as it is for many other properties.

Non-Totally Symmetric Vibrations: The Origin of the "Mystery Band" A. The vibrational origin of the A band was not found in the calculation of totally symmetric Franck–Condon factors. This is not surprising as a vibration of 3320 cm^{-1} could only be a rather high-frequency C–H stretch, and this was one of the reasons why the A band was originally thought to be due to a separate electronic transition. The bridge C–H stretching is an unlikely candidate due to a normally much lower C–H frequency (<3000 cm^{-1}) and to poor coupling with the π–π^* excitation to gain the prerequisite intensity necessary for observation. Further, the aromatic C–H stretching frequency should shift markedly upon deuteration, a fact not borne out by experiment: The observed difference of the ^1L_b and A band origins is only 20 cm^{-1} (**1**, 3320 cm^{-1}; **1**-d_{10}: 3300 cm^{-1}).

As suggested tentatively in a preliminary communication,[11] two quanta of a nontotally symmetric vibration could form the origin of the A band. Nontotally symmetric modes have intensity only in even quanta if vibronic coupling to electronic states of different symmetry is negligible. Hence, the first quantum (the fundamental) is not allowed, yet all even quanta are, and the observed vibrational levels will have the symmetry of the 0–0 level. The region in the polarized excitation spectrum of **1** half-way between the ^1L_b origin and the origin of the A band was searched in vain for evidence of a peak polarized perpendicular to the electronic transition moment direction. All observed features were parallel in nature, and we thus do not have direct experimental evidence for the two-quanta hypothesis. This negative result can be readily rationalized as due to the absence of significant vibronic coupling

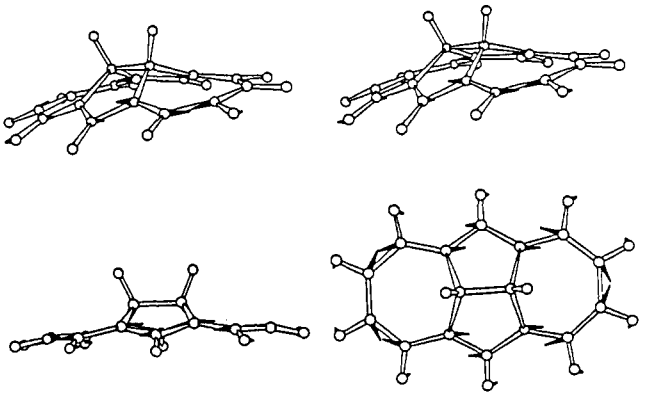

Figure 9. Normal mode $4b_2$. Top: Stereoview. Bottom: Top and side views. Darkened arrows represent atomic displacement vectors.

of the ^1L_b state, which has a fair amount of intrinsic intensity, to either the ^1L_a band, removed by about 7000 cm^{-1}, or the ^1B_a band, about 12000 cm^{-1} away.

However, the evidence provided by our calculations in favor of this assignment is quite strong. Tables VI and VII list for **1** and **1**-d_{10}, respectively, those nontotally symmetric normal modes that are calculated to contain significant calculated intensity in the second quantum of the ground to first excited singlet state transition. These vibrations cannot suffer a displacement of harmonic minima along the normal mode, and any even quantum intensity is due to a change in frequency between electronic states. One particular vibration, $4b_2$, is predicted to contain significant intensity. While the calculated absolute intensity is not as large as that observed experimentally for the A band, it clearly stands apart from all others in a relative sense. This normal mode is calculated to undergo a 149-cm^{-1} (**1**-d_{10}, 151 cm^{-1}) shift to higher frequency from the ground to the excited state. In the harmonic approximation, the observed frequency is 1660 cm^{-1} (3320/2 cm^{-1}) (**1**-d_{10}, 1650 cm^{-1} (3300/2 cm^{-1})) in the ^1L_b state. The calculated Cartesian displacements for this normal mode are presented in Figure 9. The motion is amost completely in plane and involves an alternate compression and elongation of the peripheral bonds. The vibration thus represents an oscillation between the two possible Kekulē structures of the anthracene-like perimeter. This type of annulene vibration has been referred to as a "Kekulē-type" vibration.[24]

A particularly simple description of the cyclic polyene that accounts for the frequency increase upon excitation and adequately reflects bond-length alternation starts with the two valence-bond (VB) Kekulē structures.[25,26] The potential energy surfaces for the two Kekulē structures of **1** are diagrammed in Figure 10. The horizontal coordinate is the nontotally symmetric vibrational mode $4b_2$, where r_1 and r_2 refer to the two unique bond lengths and r_0

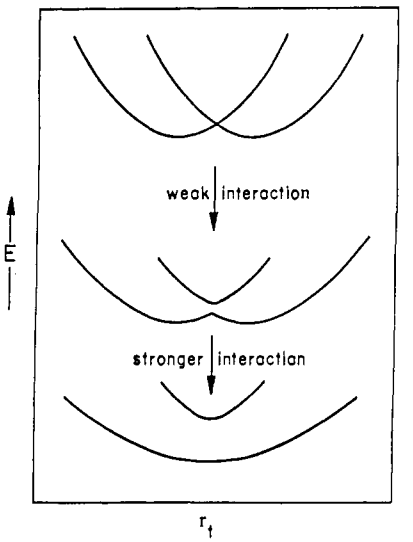

Figure 10. Valence-bond representation of the Kekulē vibration in an [*n*]annulene. Upper diagram: no interaction between Kekulē structures. Middle diagram: weak interaction expected for large *n*. Lower diagram: strong interaction expected for small *n*.

to the equal bond-length position, $r_1 = 2r_0 - r_2$. Before consideration of the resonant interaction of the VB structures, the surfaces display a parabolic shape. After the interaction, the crossing is avoided and the upper well has steeper walls. The interaction element decreases in magnitude as the ring size increases.[26] If the resonance interaction is weak enough, the lower surface can actually contain a double minimum, and in sufficiently large annulenes the ground-state bond lengths should alternate.

Conclusion

Analysis of the excitation spectrum of **1** (**1**-d_{10}) in terms of the Franck–Condon factors as measured and calculated has allowed the assignment of all observed spectral features. The fine structure of the ^1L_b band is due to totally symmetric vibrations, which represent false origins for the series-building low-frequency totally symmetric vibration most directly involving motion along the transannular interaction coordinate. It is proposed that this vibration is a manifestation of the transannular interaction that is responsible for many of the properties observed in this class of molecules. The first overtone of a nontotally symmetric vibration is proposed to form an origin upon which the previously mysterious A band is built. This vibration is calculated to be a motion alternating the two Kekulē structures of the anthracene-like perimeter ring.

Acknowledgment. The authors at Utah acknowledge support from the U.S. National Science Foundation. We are indebted to Dr. John W. Downing for assistance with the calculations, to Dr. Juliusz G. Radziszewski for the measurement of the IR of **1** in stretched polyethylene, and to Dr. Gregory M. Wallraff for preparation of the deuterated compound.

(24) Ohno, K. *J. Mol. Spectrosc.* **1979**, *77*, 329.
(25) Salem, L. *The Molecular Orbital Theory of Conjugated Systems*; Benjamin: New York, 1972; Chapter 8.
(26) Coulson, C. A.; Dixon, W. T. *Tetrahedron* **1962**, *17*, 215.